

Zaccagnaite-3R, a new Zn-Al hydrotalcite polytype from El Soplao cave (Cantabria, Spain)

RAFAEL P. LOZANO,^{1,*} CARLOS ROSSI,² ÁNGEL LA IGLESIA,³ AND EMILIO MATESANZ⁴

¹Museo Geominero, Instituto Geológico y Minero de España, Ríos Rosas 23, Madrid 28003, Spain

²Departamento de Petrología y Geoquímica, Universidad Complutense, Madrid 28040, Spain

³Instituto de Geología Económica (CSIC-UCM), Universidad Complutense, Madrid 28040, Spain

⁴CAI de Difracción de Rayos X, Universidad Complutense, Madrid 28040, Spain

ABSTRACT

We have recently discovered significant amounts of zaccagnaite, a natural Zn-Al-CO₃ hydrotalcite in the El Soplao cave (north Spain). The El Soplao zaccagnaite is speleothemic, i.e., formed in the cave, and therefore it represents a new cave mineral. The origin of El Soplao zaccagnaite is related to the diagenesis of Zn- and Al-rich ferromanganese speleo-stromatolites, where it occurs as a pore-filling cement that likely precipitated at low temperature ($\leq \sim 11$ °C). In some stromatolite layers, the abundance of zaccagnaite crystals is large enough to enable their physical separation. This has allowed us to obtain its X-ray powder-diffraction pattern, infrared spectrum, and differential thermal/thermogravimetric profiles.

The cell parameters of the El Soplao zaccagnaite, refined from X-ray powder diffraction data are: $a = 3.06616(1)$ and $c = 22.6164(1)$ Å [$\alpha = \beta = 90^\circ$, $\gamma = 120^\circ$; $V = 184.139(1)$ Å³; $Z = 3$], consistent with a new trigonal polytype of zaccagnaite: zaccagnaite-3R. Besides, the El Soplao zaccagnaite shows some features previously unknown in natural hydrotalcites, such as octahedral-like morphologies and fluorescence zoning. Electron microprobe analyses revealed that the El Soplao zaccagnaite-3R has an unusual chemistry for natural hydrotalcites, as it is significantly more rich in Al ($Zn^{2+}/Al^{3+} = 1.6$) than the hexagonal (2H) polytype ($Zn^{2+}/Al^{3+} = 2.0$). The simplified chemical formula deduced from electron microprobe analysis is $(Zn_{0.6}Al_{0.4})(OH)_2(CO_3)_{0.2} \cdot 0.5H_2O$, where C and water were calculated by stoichiometry. The carbon content calculated by stoichiometry (2.2 wt%) is in good agreement with that measured with the electron microprobe on gold-coated samples (2.5 wt%). The presence of interlayer water and CO₃ groups was confirmed by thermogravimetric analysis coupled to mass spectroscopy, and by the analysis of the infrared spectrum.

Keywords: Zaccagnaite, hydrotalcite, speleothem, El Soplao, Cantabria

INTRODUCTION

Hydrotalcites, also called anionic clays, represent a relatively rare and not very well-known group of clay minerals. However, their study is becoming increasingly important for practical purposes: their synthetic counterparts, known as layered double hydroxides, have important industrial applications, especially in catalysis (Othman et al. 2009), water treatment (Douglas et al. 2010), and human health (del Hoyo 2007).

Hydrotalcites are formed by positively charged, octahedral brucite-like layers alternating with layers of charge-balancing anions such as carbonate, sulfate, and others. The general formula of the octahedral layers is $[M_1^{2+}_x M_2^{3+}_x (OH)_2]^{x+}$, where M^{2+} can be Ca²⁺, Mg²⁺, Zn²⁺, etc. and M^{3+} can be Al³⁺, Fe³⁺, Ni³⁺, etc. Typically, x ranges between 0.17 and 0.33 (Frost et al. 2005). However, in some species this range is larger, especially in Al-hydrotalcites where x may vary between 0.14 and 0.80 (Tumiaty et al. 2008). The hydrotalcite minerals usually show two polytypic modifications, trigonal (3R-6R) and hexagonal (1H-2H-3H) (Bookin and Drits 1993), with monoclinic (1M) polytypes being rare (Martini 1980a; Krikovichev et al. 2010a).

Zaccagnaite is a Zn-Al-CO₃ natural hydrotalcite discovered in Carrara, Italy (Merlino and Orlandi 2001). The Carrara zaccagnaite corresponds to the 2H polytype (space group: $P6_3/mmc$) and has a $M^{2+}:M^{3+}$ (i.e., $Zn^{2+}:Al^{3+}$) ratio of 2:1 ($x = 0.33$) (Merlino and Orlandi 2001). The original description of zaccagnaite-2H was based on scarce, micrometric-sized crystals, and its X-ray diffraction pattern was obtained with a Gandolfi camera (Merlino and Orlandi 2001). Thus, important data such as the X-ray powder-diffraction pattern, thermogravimetry, or the infrared spectrum of zaccagnaite are still unknown. The presence of zaccagnaite has been also reported in St. Constantine, Greece (Witzke and Raade 2000), but no further structural or chemical data were provided.

We have recently discovered significant amounts of zaccagnaite in the El Soplao cave (north Spain). The El Soplao zaccagnaite is a speleothem, i.e., formed in a cave, and therefore it represents a new cave mineral. The origin of El Soplao zaccagnaite is related to the diagenesis of Zn- and Al-rich ferromanganese speleo-stromatolites, where it occurs as a pore-filling cement. The zaccagnaite-hosting stromatolites were induced by Mn-oxidizing microbes in a karstic cave stream passage, and represent the first reported occurrence of stromatolites formed in the deep interior of a cave (Rossi et al. 2010). In some stromato-

* E-mail: r.lozano@igme.es

lite layers, the abundance of zaccagnaite crystals is large enough to enable their concentration in a relatively pure form. This has allowed us to obtain its X-ray powder diffraction pattern, infrared spectrum, and differential thermal/thermogravimetric profiles, which are reported here. X-ray diffraction data indicate that the El Soplao zaccagnaite is the trigonal-3R (space group: $R\bar{3}m$) polytype, and therefore it represents a new polytype of zaccagnaite. Besides, the El Soplao zaccagnaite crystals show some features previously unknown in natural hydrotalcites. Also, electron microprobe analyses revealed that the El Soplao zaccagnaite-3R has an unusual chemistry for natural hydrotalcites, as it is significantly more rich in Al than the zaccagnaite-2H polytype described by Merlino and Orlandi (2001).

METHODS

The presence of zaccagnaite in some stromatolite samples was initially noticed via bulk powder X-ray diffraction (XRD), using a X'Pert PRO apparatus of Panalytical with a copper tube, and a graphite monochromator and automatic divergence slit, at the IGME (Geological Survey of Spain) laboratories. Identifications were made using X'Pert High Score software of Panalytical and the PDF-2 (ICDD) database. Zaccagnaite-rich stromatolite samples were cut into 2.5 cm × 4 cm blocks that were subsequently dried with acetone and vacuum-impregnated with blue-dyed epoxy. Double-polished thin sections were cut from the impregnated blocks. The thin sections were examined and imaged using a petrographic microscope equipped with UV epi-illumination. Freshly broken surfaces of selected samples were observed using a JEOL 6400 scanning electron microscope (SEM) equipped with an energy-dispersive X-ray microanalyzer. Some images were collected in a Jeol JSM-6335F field-emission SEM.

Chemical analyses of zaccagnaite crystals and the Mn-oxide-rich matrix were performed on graphite-coated polished thin sections using a JEOL JXA 8900 electron microprobe (EMP), operating at 15 kV, 20 nA, and 10 µm beam diameter. Detection limits are approximately 500 ppm for Zn, 100 ppm for Al, 290 ppm for Mn, 260 ppm for Fe, 60 ppm for Si, 70 ppm for Mg, 100 ppm for K, 140 ppm for Pb, 115 ppm for Ca, 300 ppm for Co, and 300 ppm for Ba. The standards used were gahnite (Zn), sillimanite (Al), MnO₂ (Mn), almandine (Fe), microcline (Si and K), kaersutite (Mg and Ca), vanadinite (Pb), NiCrCo (Co), and witherite (Ba). Oxygen was measured with the electron microprobe on carbon-coated polished thin sections using a LDE1 multilayer diffracting crystal, yielding a statistical precision similar to heavier elements. However, in individual analyses we observed a decrease in counts per second of oxygen through time, which we assigned to the loss of interlayer water resulting from damage of the sample by the electron beam. Fortunately, metal ratios were fairly stable during analysis, therefore the measured Zn and Al contents are considered to be reliable. Increasing the spot size would have minimized sample damage but, given the relatively small size of the zaccagnaite crystals, we chose to keep the spot size at 10 µm. The standard used for O is gahnite. Carbon was measured with the electron microprobe on gold-coated polished thin sections using the same multilayer diffracting crystal and dolomite as the standard for C.

Bulk zaccagnaite-rich samples were gently crushed and then sieved to obtain a grain size between 0.1 and 0.2 mm. In this fraction, zaccagnaite was separated from the ferromanganese-oxide matrix using a Frantz magnetic separator. Visible non-magnetic impurities (mostly quartz and nordstrandite) were removed manually from the zaccagnaite-rich fraction using a thin brush and a binocular lens.

For the refinement of cell parameters and structure, a portion of purified zaccagnaite sample was mounted in a 0.3 mm diameter capillary. The scan was collected in transmission mode in a Panalytical X'Pert PRO diffractometer with a Cu tube working at 45 kV and 40 mA, a hybrid primary monochromator (parallel beam with $\lambda = 1.5406 \text{ \AA}$) and a fast RTMS detector working in scanning mode. Data were collected in the 2θ range 5 to 100°, with a step size of 0.017° and an equivalent time per step of 1500 s (total scan time of 19 h approximately).

Thermal decomposition was carried out using a SDT Q 600 instrument, coupled to a Thermo Star quadrupole mass spectrometer for gas analysis. Twelve milligrams of purified zaccagnaite were heated in an open platinum crucible at a rate of 10 °C min⁻¹ up to 1000 °C in a flowing argon atmosphere (100 mL min⁻¹). The gases analyzed were O₂, H₂O, and CO₂. A portion of the purified zaccagnaite sample was used to obtain its Fourier-transform infrared (FTIR) spectrum, which was recorded using the KBr tablet technique (1 wt% sample) on a Nicolet Magna

IR-750 spectrometer. 128 scans were taken to improve the signal to noise ratio in the range of 400–4000 cm⁻¹, and the normal resolution was 4 cm⁻¹.

Unless otherwise specified, all data were collected using instruments at the Universidad Complutense, Madrid (Spain).

RESULTS

Occurrence and paragenesis

The zaccagnaite crystals described here occur within Al- and Zn-rich ferromanganese deposits from El Soplao cave. These deposits are located in the main passage of the cave, where they form stromatolites interbedded with siliciclastic sediments (for details, see Rossi et al. 2010). The zaccagnaite crystals are partially filling the primary porosity of some dendritic stromatolite layers (Figs. 1a–1c). The presence of zaccagnaite is restricted to layers in which the ferromanganese oxide material is relatively rich in Zn, i.e., above 15 wt%. In the zaccagnaite-bearing stromatolite layers, the average chemical composition of the ferromanganese-oxide-rich material (wt%) is: Zn 15.74, Mn 16.13, Fe 4.62, Al 7.24, Pb 1.97, Si 1.06, Ca 0.54, Mg 0.20, Co 0.11, and Ba 0.05 (n = 25). In the stromatolite layers in which the ferromanganese-oxide-rich material is relatively poor in Zn (range: from 4.59 to 14.03 wt%), no zaccagnaite is observed. The ferromanganese-oxide-rich material hosting the zaccagnaite is mostly XRD amorphous, but their FTIR spectra are consistent with the predominance of birnessite and in individual cases of rancieite (Rossi et al. 2010). Apart from zaccagnaite, other authigenic minerals that are partially filling the porosity of the ferromanganese deposits are nordstrandite, woodruffite, calcite, dolomite, and aragonite. Illite, kaolinite, quartz, and zircon are also common in the ferromanganese deposits, but they are detrital in origin.

As seen in backscattered electron (BSE) images, the ferromanganese-oxide-rich material shows an alteration halo where it is in contact with zaccagnaite crystals (Fig. 1c). Electron microprobe analyses revealed that the alteration halo is depleted in Mn, Zn, and Al and enriched in Fe, in relation to the unaltered oxides.

Appearance and physical properties

The zaccagnaite crystals are translucent, white to pale yellow, and have white streak and adamantine luster. Perfect cleavage is observed in broken specimens and especially in polished surfaces slightly etched with 2% formic acid. Density could not be measured directly, but it was calculated to be 2.82 g/cm³ taking into account the molecular mass deduced from the chemical formula and the unit-cell volume deduced from XRD data (see below).

As revealed by SEM examination, the zaccagnaite crystals show both octahedral and hexagonal forms. Some octahedral forms are regular (Figs. 2a–2b) and some are non-regular (Fig. 2c). The hexagonal forms consist of pyramids (Fig. 2d) and short prisms (Fig. 2e), with local intergrowth of thin plates (Fig. 2f). In some cases, the hexagonal crystals are in mutual contact with the octahedral crystals, and locally both forms are interpenetrated (Fig. 2c). Locally, the zaccagnaite crystals are skeletal (Fig. 2g). Crystal size ranges between 10 and 70 µm (usually 10–30 µm), a range typical of hydrotalcites (Frost and Erickson 2004).

Most zaccagnaite crystals contain inclusions of illite (Fig. 3a) and more rarely of nordstrandite (Fig. 3b). The illite inclu-

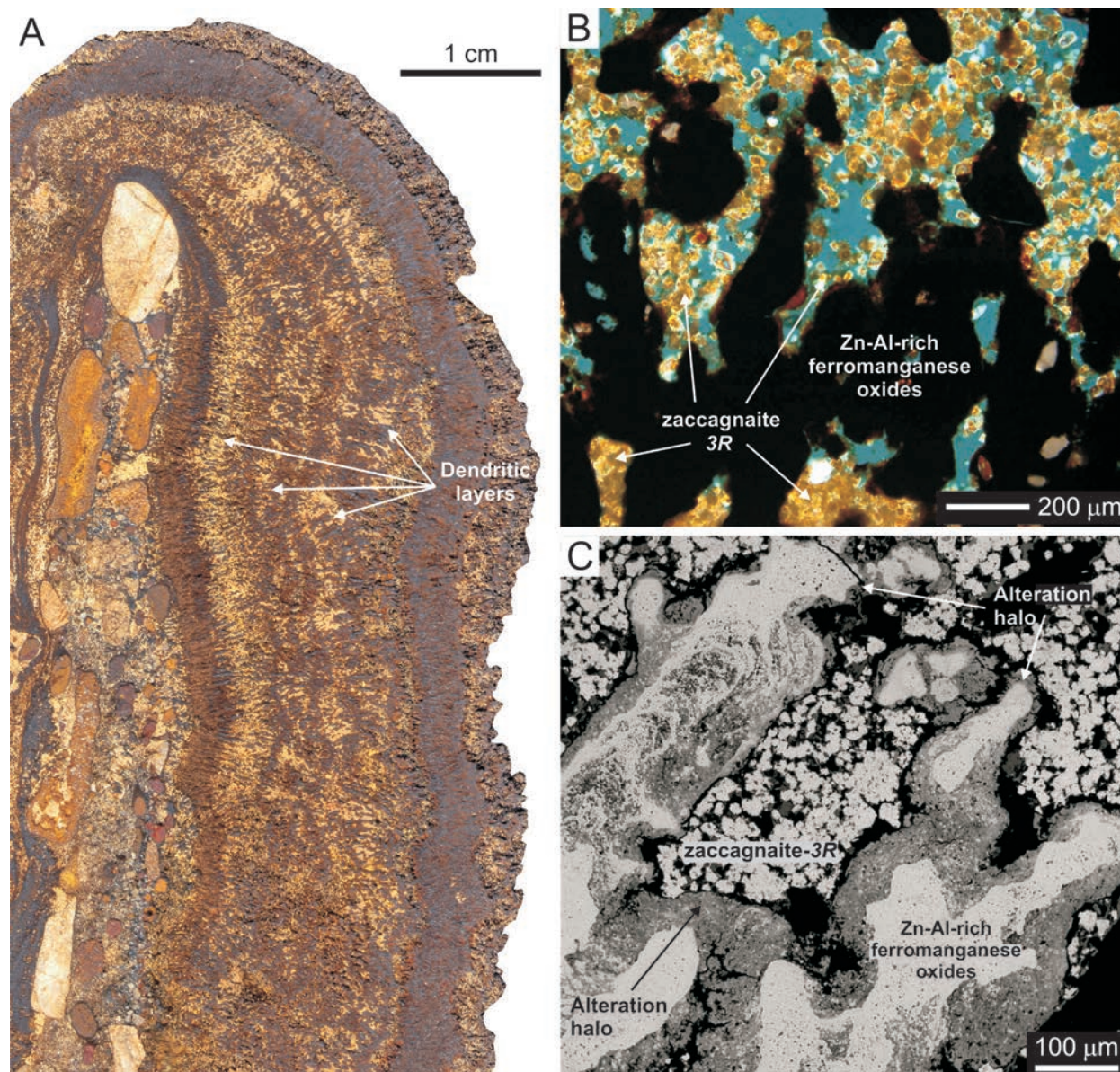


FIGURE 1. (a) Fe-Mn stromatolite section showing the alternation of dendritic and laminar layers. (b) Dendritic stromatolite layers composed of Zn-Al-rich ferromanganese oxides. The zaccagnaite-3R crystals are partially filling the primary porosity. Thin section, semi-crossed polars. (c) alteration halo between the zaccagnaite-3R crystals and the Zn-Al-rich ferromanganese oxides. BSE image.

sions are locally aligned along growth bands (Fig. 3c). The illite inclusions are more abundant in the larger pores, where clay has penetrated more easily, supporting a detrital origin for the illite. Inclusion-free crystals of zaccagnaite are also present, but they are much less common (Fig. 3d). They are found only in small pores (50–200 μm), where the access of detrital illite was much more restricted.

Zaccagnaite is optically uniaxial negative. In thin sections of standard thickness (30 μm), the zaccagnaite crystals show very high interference colors, comparable to those in carbonates (Figs. 4a–4b).

Under UV epi-illumination (360–370 nm), some crystals of zac-

cagnaite show bluish to yellowish fluorescence (FL). FL is normally restricted to hairline bands that define concentric growth bands (Fig. 4c). Electron microprobe traverse lines across zoned crystals have not revealed significant chemical variation.

X-ray crystallography

Initially, the qualitative analysis of the XRD scan of the purified zaccagnaite sample was performed by comparison with the minerals subset of the ICDD PDF database. This analysis indicated that the sample consisted of a mixture of nordstrandite [Al(OH)₃] and an unidentified mineral, with quartz as minor phase. Subsequently, the search was extended to the

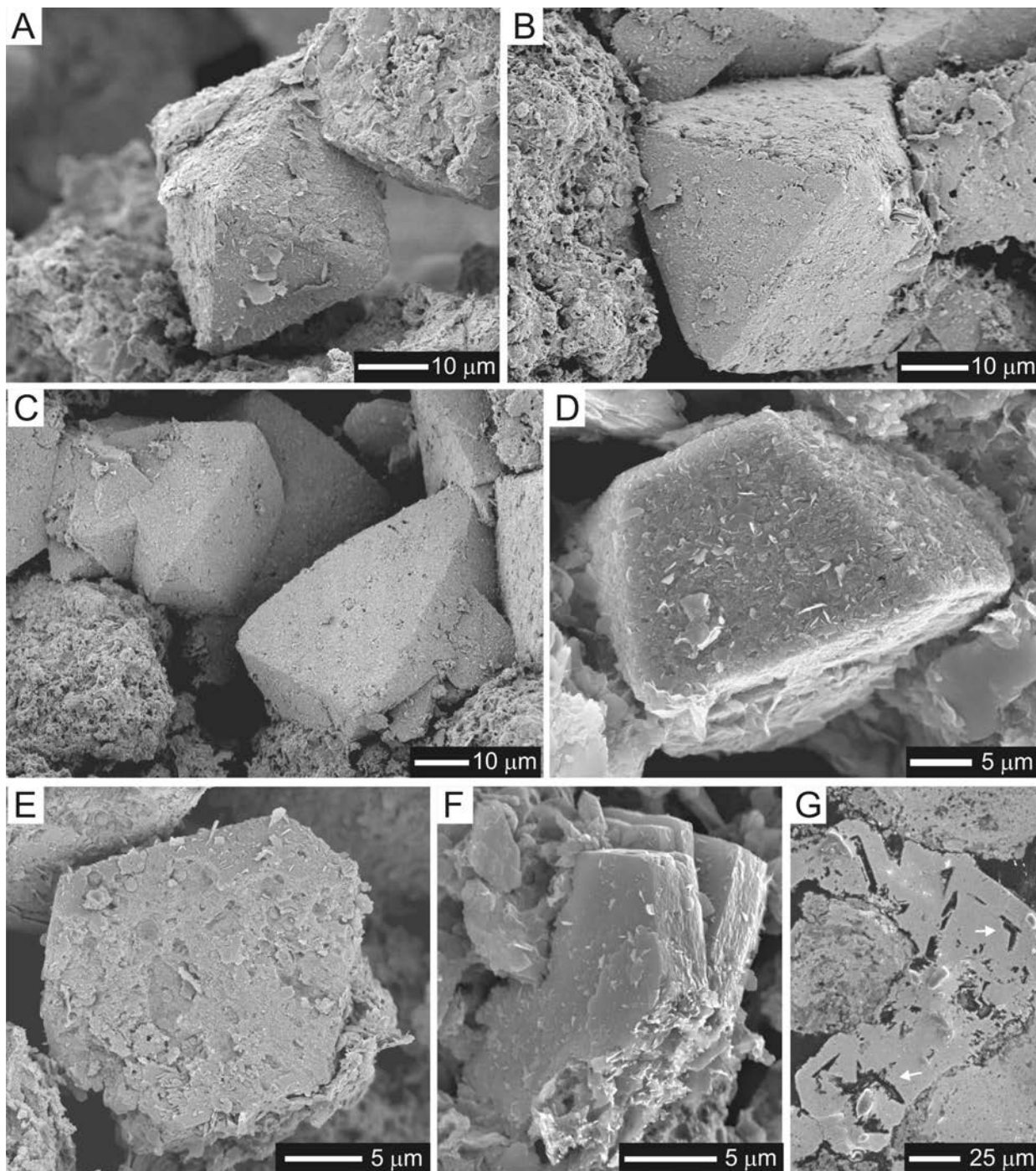


FIGURE 2. Morphology of zaccagnaite-3R crystals. (a–b) Regular octahedral forms; (c) irregular octahedral forms; (d) hexagonal pyramid; (e–f) hexagonal short prisms. SEM images of broken specimens. (g) Skeletal crystals. BSE image.

inorganic subset, resulting that the unidentified mineral peaks were matched by a synthetic Zn-Al layered double hydroxide (ICDD card 01-075-2983) described by Lombardo et al. (2005). This phase corresponds to the hydrotalcite-like 3R polytype of the Zn-Al hydroxide carbonate hydrate, of which zaccagnaite (Merlino and Orlandi 2001) is the 2H polytype with equivalent chemical composition. Therefore, the analyzed phase represents

the 3R polytype of the mineral zaccagnaite.

The El Soplao zaccagnaite-3R structure was refined by the Rietveld method (Rietveld 1967, 1969) with the program Fullprof (Rodríguez-Carvajal 1993). The starting model for zaccagnaite-3R was the structure of the synthetic counterpart as reported in the entry 155052 of the ICSD database (Belsky et al. 2002). The sample was fully described by including structural data for

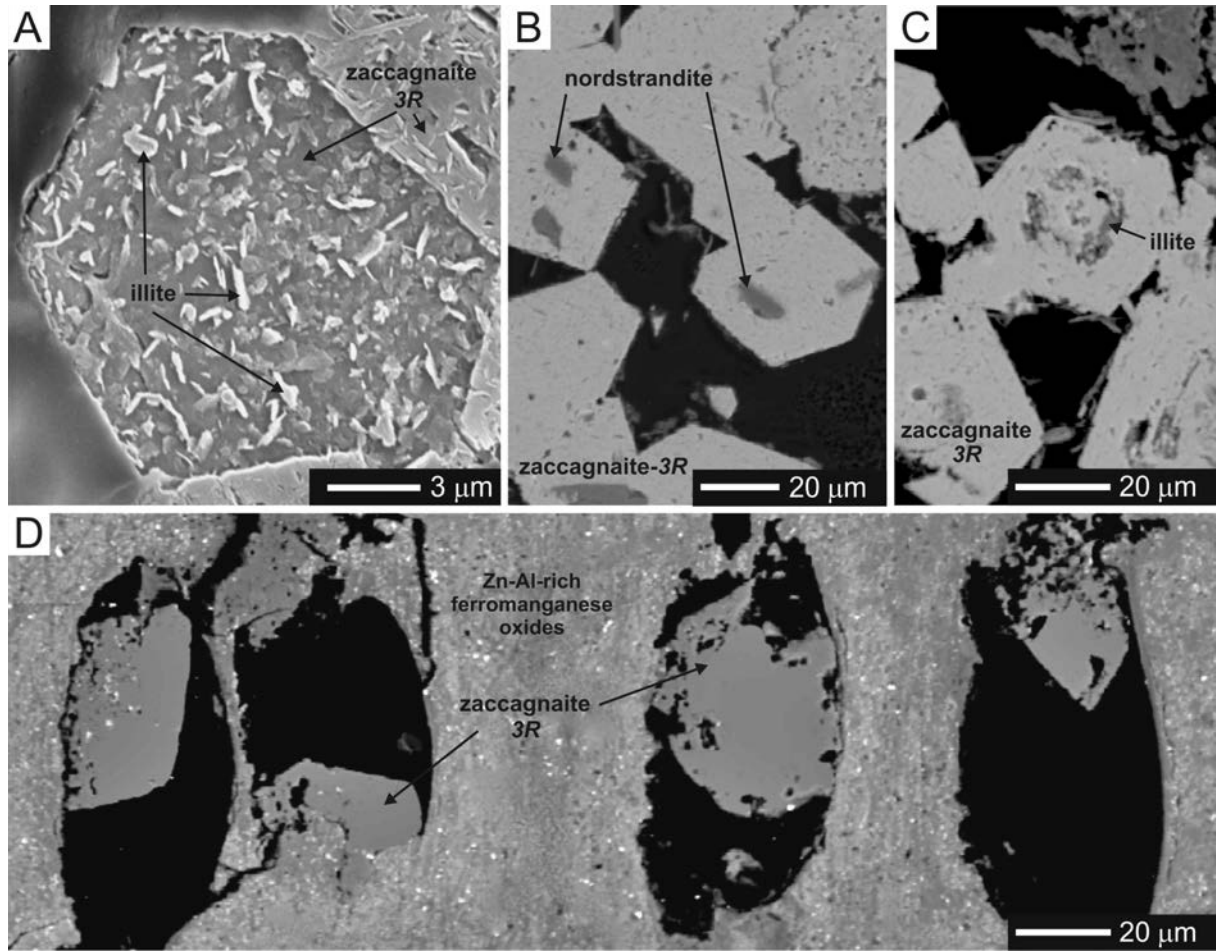


FIGURE 3. (a) Illite inclusions in hexagonal zaccagnaite-3R. Polished surface slightly etched with 2% formic acid. SEM image. (b) Nordstrandite inclusions in hexagonal zaccagnaite-3R. (c) Illite inclusions in concentric growth bands of hexagonal zaccagnaite-3R. (d) Inclusion-free crystals of zaccagnaite-3R in small pores. (b–d) BSE image.

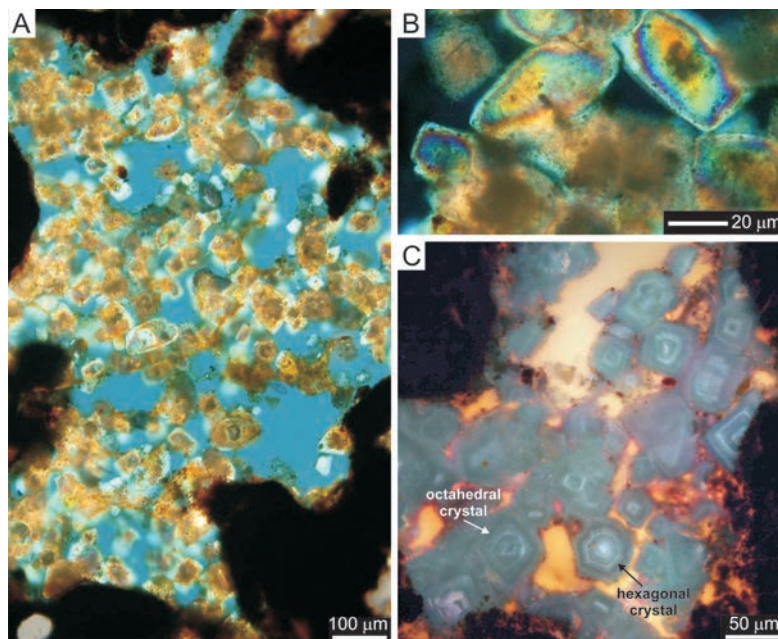


FIGURE 4. (a–b) Zaccagnaite-3R crystals in thin section (semi-crossed polars). (c) Octahedral and hexagonal crystals of zaccagnaite-3R showing luminescent concentric growth bands. Thin section, UV epi-illumination. The yellow areas represent epoxy-filled porosity. The background green fluorescence of the zaccagnaite-3R crystals is caused by the mounting media (adhesive Loctite 358).

nordstrandite (entry 16018) and quartz (entry 174). Zaccagnaite-3R was refined for structural and thermal parameters, while keeping B_{iso} for C and H fixed, and introducing a coordinate constraint for H based on O-H interatomic distance to avoid instabilities in the refinement process. Site occupation factors were fixed to the values given by chemical analysis (see the chemistry section below), except for water oxygen occupancy that was refined getting a result of 0.456(2) water molecules per cation, close to the value of 0.5 normally assumed for hydrotalcites. The final refinement agreement factors are shown in Table 1 along with the structural parameters obtained for zaccagnaite-3R. The CIF structural file obtained for zaccagnaite-3R and the zaccagnaite-3R reflections list are on deposit¹. Figure 5 shows the calculated and observed powder XRD profiles of the purified zaccagnaite-3R sample.

Chemistry

A total of 182 individual microprobe analyses were performed on zaccagnaite-3R crystals from three different samples (Table 2, average 3). Most analyses (150) are from crystals with illite inclusions, as indicated by the presence of significant and variable Si and K contents and confirmed by SEM and BSE images (Figs. 3a–3c). In these analyses, the strong co-variation between Si and K ($R^2 = 0.8$) (Fig. 6), further confirms the presence of variable amounts of illite.

Fortunately, in 32 microprobe analyses K is below detection limit (DL $\sim 0.01\%$) and Si is insignificant, indicating the absence of illite (Table 2, averages 1 and 2). BSE imaging further confirms this conclusion (Fig. 3d). Among the illite-free analyses, eight of them are selected as the most representative because their totals (calculated by stoichiometry) are between 98.5 and 102.5% (Table 2). In the eight illite-free representative analyses, the average divalent/trivalent cation ratio (i.e.,

Zn^{2+}/Al^{3+}) is = 1.63 ($x = 0.38$).

As indicated in the Methods section, the EMP underestimates the O content of the zaccagnaite, hence the O content calculated by stoichiometry should be more accurate. In hydrotalcites, the amount of water molecules present between the octahedral layers is normally assumed to be 0.5 H₂O per cation. This would represent 8.6 wt% of interlayer water.

The C content was also calculated by stoichiometry taking into account the following. (1) Hydrotalcites are formed by octahedral layers structurally similar to brucite [Mg(OH)₂], in which a fraction of M(II) ions are replaced by M(III) ions. This replacement results in a net positive charge on the octahedral layers, which is balanced by interlayer anions. (2) EMP data indicate that, apart from carbonate, other possible interlayer anions are essentially absent (i.e., Cl, W, V, S, and P below detection limits). Therefore, there should be ½ carbonate ion for each trivalent cation (i.e., Al³⁺) in the octahedral layer. This calculation gives 2.2 wt% of C, which is in good agreement with the C content measured with the electron microprobe on gold-coated samples (2.5 wt%).

Hydrotalcites have two OH groups for each cation and ½ carbonate for each trivalent cation of the brucite-like layer. Therefore, the chemical formula was calculated by adding the amounts of O, H, and C required by stoichiometry to the measured amounts of Zn, Al, Mg, Mn, and Fe. Thus, 46.77 wt% O, 2.38 wt% H, and 2.17 wt% C were added to give 2(OH), 0.19(CO₃), and 0.5(H₂O) in the chemical formula: this raises the analytical

¹ Deposit item AM-12-023, CIF and zaccagnaite-3R reflections list. Deposit items are available two ways: For a paper copy contact the Business Office of the Mineralogical Society of America (see inside front cover of recent issue) for price information. For an electronic copy visit the MSA web site at <http://www.minsocam.org>, go to the *American Mineralogist* Contents, find the table of contents for the specific volume/issue wanted, and then click on the deposit link there.

TABLE 1a. XRD data of zaccagnaite-3R

Global and phase agreement factors	Structural parameters		Interatomic distance (Å)	
R_p	5.23	Space group $R\bar{3}m$	O1-Zn1/Al1	2.030(1)
R_{wp}	6.97	a (Å)	O1-H1	1.13(5)
R_{exp}	5.12	c (Å)	C1-O2	1.165(7)
χ^2	1.85	V (Å ³)		184.139(1)
R_{Bragg}	3.00	Z		3
R_t	3.04			
Fraction (%)	45.8(4)			

TABLE 1b. XRD data of zaccagnaite-3R

Atom label	Type	Mult	Wyck	Atomic coordinates			B_{iso}	SOF
				x	y	z		
Zn1	Zn	3	a	0.0	0.0	0.0	1.42(5)	0.6
Al1	Al	3	a	0.0	0.0	0.0	1.42(5)	0.4
O1	O	6	c	0.0	0.0	0.3772(1)	1.68(8)	1
H1*	H	6	c	0.0	0.0	0.427(2)	1.68	1
C1†	C	6	c	0.3333	0.6667	0.502(3)	2.5	0.1
O2	O	18	h	0.114(1)	-0.114(1)	0.499(2)	2.5(5)	0.1
Wat	O	18	h	0.114(1)	-0.114(1)	0.499(2)	2.5(5)	0.076(2)

* Refined with position restrain based on O-H distance and B_{iso} fixed.

† Refined with B_{iso} fixed.

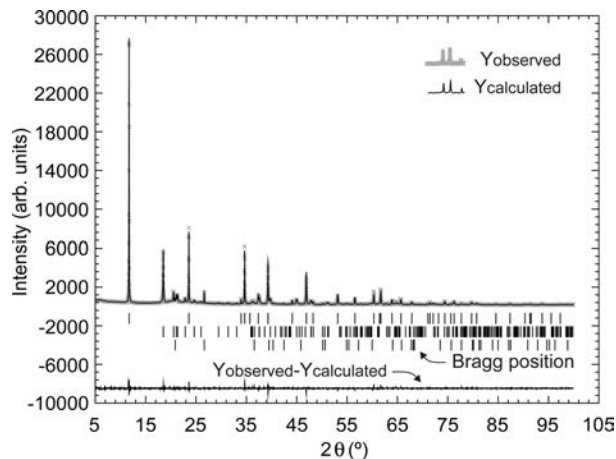


FIGURE 5. Comparison between the calculated and experimental powder XRD profiles of zaccagnaite-3R. Tick marks under the scan correspond to reflections for zaccagnaite-3R, nordstrandite, and quartz (top down).

TABLE 2. Microprobe zaccagnaitite-3R analyses (wt%)

	Representative illite-free analyses (wt%)							Averages			
	1	2	3	4	5	6	7	1	2	3	
Zn	36.6(3)	35.7(3)	36.1(9)	36.4(3)	37.9(3)	38.0(3)	37.3(3)	37.1(3)	36.89(8)	36(2)	36(2)
Fe	0.23(3)	0.29(3)	0.25(3)	0.26(3)	0.24(3)	0.22(3)	0.19(3)	0.13(3)	0.23(5)	0.3(1)	0.8(4)
Mg	0.34(2)	0.32(2)	0.33(2)	0.33(2)	0.32(2)	0.43(2)	0.28(2)	0.34(2)	0.34(4)	0.31(5)	0.35(8)
Mn	0.45(4)	0.53(5)	0.43(4)	0.43(4)	0.44(4)	0.40(4)	0.35(4)	0.32(4)	0.42(6)	0.41(9)*	0.3(2)†
Al	9.57(7)	9.90(7)	9.82(7)	9.85(7)	10.16(7)	9.89(7)	9.56(7)	9.41(7)	9.8(2)	9.7(5)	10.1(5)
Si	0.04(1)	0.05(1)	<0.01	<0.01	<0.01	0.01(1)	0.03(1)	0.02(1)	0.02(2)	0.09(8)	0.9(8)
K	<0.01	0.01(1)	<0.01	<0.01	<0.01	<0.01	<0.01	<0.01	<0.01	<0.01	0.1(1)
O	40.3(6)	37.0(6)	36.3(7)	35.2(7)	36.2(7)	37.1(2)	39.7(2)	39.4(2)	38(2)	38(2)	39(3)
Total	87.6	83.8	83.2	82.5	85.3	86.0	87.4	86.7	85(2)	86(3)	88(4)
Div/Triv	1.66	1.57	1.59	1.60	1.61	1.66	1.67	1.69	1.63	1.63	1.56
x	0.38	0.39	0.39	0.38	0.38	0.38	0.37	0.37	0.38	0.38	0.39

Notes: Div/Triv = $(Zn^{2+}+Fe^{2+}+Mg^{2+}+Mn^{2+})/Al^{3+}$. $x = Al^{3+}/(Zn^{2+}+Fe^{2+}+Mg^{2+}+Mn^{2+}+Al^{3+})$. Averages: 1 = illite-free representative analyses (n = 8); 2 = total illite-free analyses (n = 32; *n = 18); 3 = total analyses (n = 182; †n = 39).

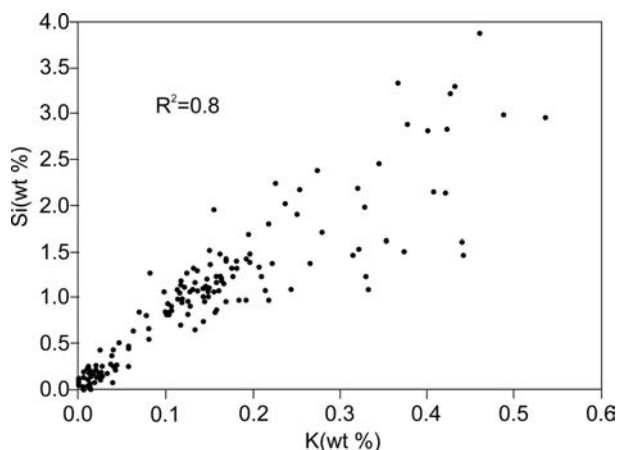


FIGURE 6. Co-variation between Si and K of zaccagnaitite-3R from electron microprobe (EMP) data (n = 182; $R^2 = 0.8$).

total to 99.02 wt%. By recalculating to 100.00 wt%, the corresponding chemical formula, on the basis of $Zn+Fe+Mg+Mn+Al = 1$ is: $(Zn_{0.593}Fe_{0.004}Mg_{0.015}Mn_{0.008}Al_{0.380})(OH)_2(CO_3)_{0.19} \cdot 0.5H_2O$ or, in simplified formula, $(Zn_{0.6}Al_{0.4})(OH)_2(CO_3)_{0.2} \cdot 0.5H_2O$. Expressed as oxides, this formula transforms into: 46.18 wt% ZnO, 0.29 wt% FeO, 0.54 wt% MgO, 0.54 wt% MnO, 18.56 wt% Al_2O_3 , 26 wt% H_2O , and 8.01 wt% CO_2 .

Thermal analysis

The differential thermal analysis (DTA) and thermogravimetry (TG) curves of El Soplao zaccagnaitite-3R, which also included some nordstrandite as indicated above, are shown in Figure 7a. The relative ion currents of CO_2 , H_2O , and O_2 , together with the derivative thermogravimetry (DTG) are shown in Figure 7b. These diagrams are similar to those obtained by Frost et al. (2005) from thermal decomposition of Zn-substituted takovite $Zn_6Al_2CO_3(OH)_6 \cdot 4H_2O$, a synthetic hydroxalite with chemical composition similar to zaccagnaitite.

The total mass loss is around 35%. As deduced from the thermal curves, the decomposition of the mineral occurs in two main steps (Figs. 7a–7b). The first step involves the loss of CO_2 (at $\sim 185^\circ C$) and hydration water (at $\sim 190^\circ C$), resulting in a mass loss of $\sim 6\%$. The second step also involves the loss of H_2O (at $\sim 266^\circ C$) and CO_2 (at $\sim 281^\circ C$), resulting in a mass loss of $\sim 25\%$. This second step is attributable to dehydroxylation followed by decarbonation. Although most CO_2 is lost below 400

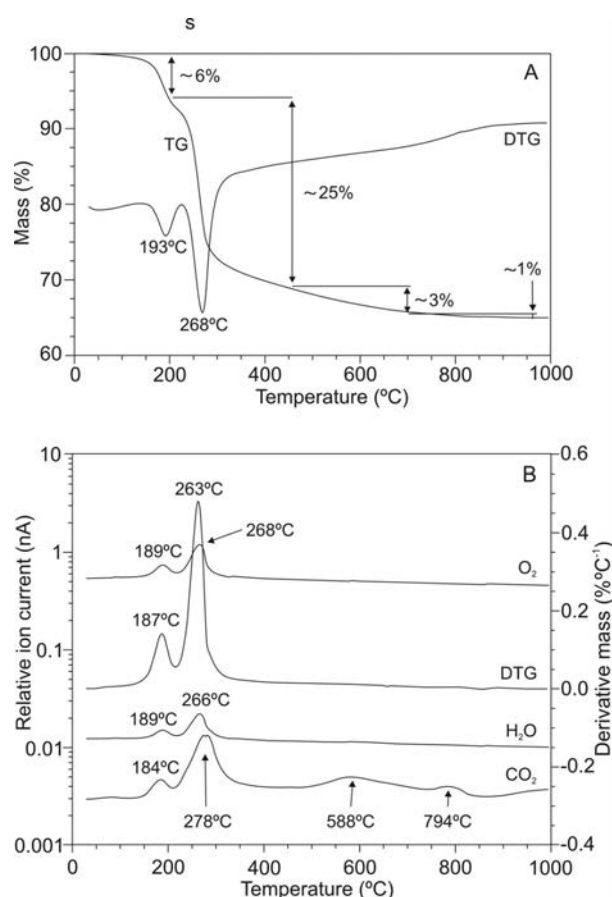


FIGURE 7. (a) Differential thermal analysis (DTA) and thermogravimetry (TG) curves of zaccagnaitite-3R (plus nordstrandite). (b) Relative ion currents of CO_2 , H_2O , and O_2 , together with the derivative thermogravimetry (DTG).

$^\circ C$, the ion current curve (Fig. 7b) indicates small losses at 588 and 797 $^\circ C$, corresponding to the slight mass loss shown by the TG curve between 430 and 900 $^\circ C$ (~ 3 and $\sim 1\%$, respectively).

FTIR spectrum

In the FTIR spectrum of the El Soplao zaccagnaitite-3R purified sample, hydrogen stretching vibrations can be identified at 3700–3300 cm^{-1} (Vieira et al. 2009; Dani et al. 2001). Peaks in

this region (at 3621, 3564, 3527, 3500, 3425, and 3360 cm^{-1}) correspond to both zaccagnaite and nordstrandite. The peak at 1625 cm^{-1} can be attributed to the bending mode of zaccagnaite-3R interlayer water (Fig. 8). Similar bands occurs in natural hydrotalcites (e.g., Frost et al. 2008) and synthetic Zn-Al hydrotalcites (e.g., Roto et al. 2009).

The main absorption band of the carbonate anions is observed at 1450–1300 cm^{-1} , consisting of a double peak with a broad base (main peak at 1355 cm^{-1} ; Fig. 8), which corresponds to the ν_3 vibration mode (doubly degenerate asymmetric stretching). Also, the bands corresponding to the ν_4 bending mode of carbonate anions are observed at 775, 708, and 674 cm^{-1} and the ν_1 carbonate symmetric stretching vibration mode occurs at 1063 cm^{-1} . The out-of-plane bending mode (ν_2) is obscured in the El Soplao zaccagnaite spectrum, due to a strong overlap with the vibrational modes of the hydroxide sheets, as is characteristic in natural and synthetic Zn-Al hydrotalcites (Frost and Reddy 2006; Klopogge et al. 2004).

The complexity of the spectrum in the 1100–400 cm^{-1} region is shown in Figure 8, where the overlapping of bands makes the assignment of peaks difficult. Four broad compound bands are observed at: 1100–900 cm^{-1} (peaks at 1063, 1031, 1006, 975, and 918 cm^{-1}), 900–700 cm^{-1} (peaks at 810, 775, and 708 cm^{-1}), 700–500 cm^{-1} (peaks at 674, 612, and 538 cm^{-1}), and 500–400 cm^{-1} (peaks at 450, 430, and 412 cm^{-1}). Similar to Mg-hydrotalcites (Klopogge and Frost 1999), the band around 538 cm^{-1} can be assigned to translation modes of hydroxyl groups influenced by the presence of Al^{3+} in both zaccagnaite-3R and nordstrandite. The corresponding deformation modes can be identified at 918, 1006, and 1031 cm^{-1} . The peak at 612 cm^{-1} may correspond to the hydroxyl translation mode influenced by the presence of Zn^{2+} . The peaks at 412, 430, and 450 cm^{-1} may correspond to librational modes of interlayer water molecules (Wang et al. 2003), but the latter peak may also correspond to symmetric vibrations of the Al-OH bond (Vieira et al. 2009).

DISCUSSION

The zaccagnaite-3R structure refined from powder XRD data of the El Soplao zaccagnaite corresponds to the $R\bar{3}m$ space group

of the trigonal crystal system (Table 1) and there is good agreement between the calculated and observed powder XRD profiles of the sample (Fig. 5). The stacking spacing in the El Soplao zaccagnaite ($c = 22.6164 \text{ \AA}$) results from a three-hydroxide-layer stacking sequence whereas only two layers are involved in the 2H zaccagnaite polytype from Carrara ($c = 15.114 \text{ \AA}$; Merlino and Orlandi 2001). Therefore, the El Soplao zaccagnaite represents a new polytype of this mineral, to be denoted zaccagnaite-3R. Nevertheless, the basic structural element in this mineral is the same as described by Merlino and Orlandi (2001) for the 2H polytype: a repetitive unit formed by a brucite-like layer containing the Zn/Al octahedra and an interlayer of carbonate anions and water. There are some chemical differences between both polytypes due to the higher Al content in the zaccagnaite-3R and the consequentially higher carbonate incorporation to the interlayer to compensate the charge excess. Interlayer oxygen atoms are located in three symmetry equivalent positions with low occupancy factor, being part of either the carbonate groups or the water molecules. The X-ray powder-diffraction profile of El Soplao zaccagnaite is the first reported for a natural Zn-Al carbonate hydrotalcite.

The EMP results indicate that the $\text{Zn}^{2+}/\text{Al}^{3+}$ ratio of the El Soplao zaccagnaite-3R approaches 1.6 (Table 2), contrasting with most natural hydrotalcites, in which the cationic divalent to trivalent ratio is ≥ 2.0 (e.g., Taylor 1973; Bish and Brindley 1977; Taylor et al. 1991; Ashwal and Cairncross 1997; Merlino and Orlandi 2001). Also, the El Soplao zaccagnaite-3R is significantly more rich in Al than the zaccagnaite-2H polytype, which has a $\text{Zn}^{2+}/\text{Al}^{3+}$ ratio of 2 (Merlino and Orlandi 2001). Such a difference in Zn:Al ratio between the 2H and 3R polytypes is probably linked to different degrees of ordering of the metal cations (S. Merlino, pers. comm.): while some ordering may be present in the 2H polytype (Merlino and Orlandi 2001), no evidences of such ordering are observed in the 3R polytype.

Traditionally, it was believed that the minimum divalent to trivalent ratio in hydrotalcites was 2, due to crystal-chemistry considerations (Brindley and Kikkawa 1979; Trave et al. 2002). However, synthetic hydrotalcites may show lower ratios, including the Zn-Al varieties that can have $\text{Zn}^{2+}/\text{Al}^{3+}$ ratios as low as

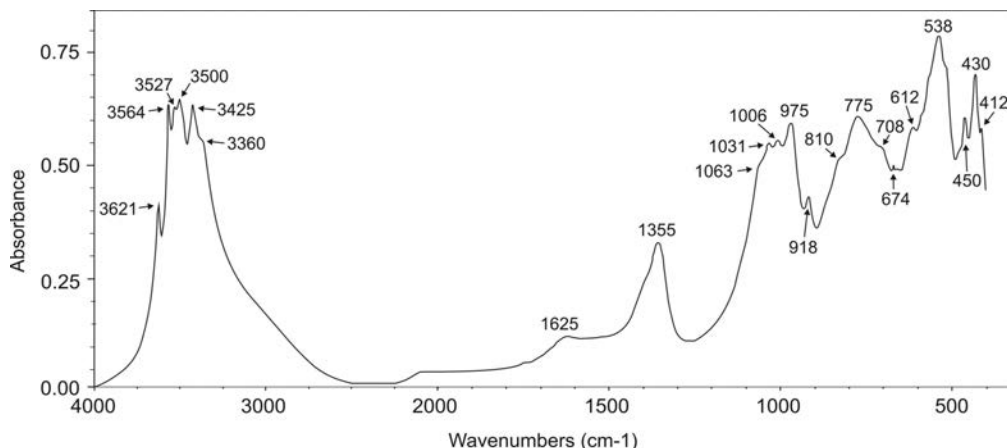


FIGURE 8. Infrared spectra of zaccagnaite-3R (plus nordstrandite) in the 400 to 4000 cm^{-1} region.

~1.5 (Thevenot et al. 1989; He et al. 2006). Apart from the El Soplao zaccagnaite-3R, other natural Zn-Al hydrotalcites do show Zn^{2+}/Al^{3+} ratios of less than 2 (Table 3), namely those having sulfate as interlayer anion instead of carbonate: glaucocerinite ($Zn^{2+}/Al^{3+} = 1.6$; $x = 0.38$; Raade et al. 1985) and zincowoodwardite ($Zn^{2+}/Al^{3+} = 1.0$ – 2.0 ; $x = 0.33$ – 0.50 ; Witzke and Raade 2000). Therefore, the El Soplao zaccagnaite-3R confirms the existence of CO_3 -Zn-Al natural hydrotalcites with a Zn^{2+}/Al^{3+} ratio of less than 2, similar to the synthetic analogues and to SO_4 -Zn-Al natural hydrotalcites.

This work presents for the first time the thermogravimetric and IR data of a natural Zn-Al carbonate hydrotalcite. The calculation of the contents in OH, H_2O , and CO_2 from thermogravimetric data (Fig. 7a) is complicated, because, in the analyzed purified zaccagnaite sample, there is a significant amount of nordstrandite that could not be eliminated completely. The main loss of OH in nordstrandite occurs approximately between 270 at 300 °C (Kovács-Pálffy et al. 2008), so it overlaps with the main loss of OH in zaccagnaite (~270 °C). Probably, the decomposition products after both zaccagnaite-3R and nordstrandite are Zn-Al oxides (Frost et al. 2005; Temuujin et al. 2000). Unlike the synthetic material, El Soplao zaccagnaite-3R shows small losses of CO_2 at high temperatures (500–900 °C). In the IR spectrum, the main absorption band of the carbonate anions (ν_3 mode) can be clearly recognized at 1450–1300 cm^{-1} , although there is overlap of zaccagnaite-3R and nordstrandite bands.

The octahedral-type morphology of zaccagnaite-3R crystals (Figs. 2a–2c), is unique in natural hydrotalcites, which normally

occur either as platelets (De Vaal and Viljoen 1971; Taylor 1973; Martini 1980a, 1980b; Zamarreño et al. 1989; Witzke and Raade 2000) or as hexagonal pyramids and prisms (Rodgers et al. 1977; Drits et al. 1987; Chao and Gault 1997; Krivovichev et al. 2010a; Zhitova et al. 2010). In synthetic hydrotalcites, hexagonal forms (platelets) are also dominant (e.g., Adachi-Pagano et al. 2003; He et al. 2006), including the Zn-Al varieties (Thevenot et al. 1989; Zhao et al. 2002). However, octahedral forms have only been locally reported in synthetic Zn-Al hydrotalcites (Klopprogge et al. 2004). Therefore, the octahedral forms that are commonly observed in the El Soplao zaccagnaite-3R are clearly exceptional (Figs. 2a–2c).

The FL zonation observed in zaccagnaite-3R crystals from El Soplao (Fig. 4c) is also unique in natural hydrotalcites. Fluorescent growth bands can be correlated from octahedral crystals to hexagonal crystals (Fig. 4c), indicating that the growth of both forms was coeval. The FL zoning is not related to detectable chemical variation as measured by the EMP. Therefore the origin of the fluorescence could be related either to trace amounts (below the EMP detection limit) of inorganic FL activators (such as actinides and lanthanides, as reported by Stumpf et al. 2007 and Chen and Zhang 2010 for hydrotalcite-like compounds), or, more likely, to the incorporation of organic acids (specially fulvic acid), as it is common in other cave carbonates such as calcite and aragonite (Ramseyer et al. 1997; van Beynen et al. 2001). Besides, the presence of organic acids in the interlayer space of hydrotalcites has been shown to activate fluorescence in some synthetic examples (Su et al. 2011).

TABLE 3. Composition and reported symmetry of different hydrotalcite minerals with the general formula: $M_2^{2+}Al_x(OH)_2(A^n)_{x/n} \cdot mH_2O$

	Domin. M^{2+}	M^{2+}/Al^{3+}	$x = Al^{3+}/(Al^{3+}+M^{2+})$	A^n	Symmetry	References
hydrotalcite	Mg	3.00	0.25	CO_3	$R\bar{3}m$	1
manasseite	Mg	3.00	0.25	CO_3	$P6_3/mmc$	1
quintinite-2H	Mg	2.00	0.33	CO_3	$P6_322$	2
quintinite-3T	Mg	2.00	0.33	CO_3	$P3_12, P3_212$	2
quintinite-2H-3c	Mg	2.00	0.33	CO_3	$R32$	3
quintinite-1M	Mg	2.00	0.33	CO_3	$C2/m$	4
motukoreaite	Mg	1.32	0.43	SO_4, CO_3	$R\bar{3}m$	5
meixnerite	Mg	3.00	0.25	OH	$R\bar{3}m$	6
chlormagaluminite	Mg	2.00	0.33	Cl, CO_3	$P6/mcm, P6cm, P\bar{6}c2$	7
caresite	Fe	2.00	0.33	CO_3	$P3_12-P3_212$	2
nikischerite	Fe	2.00	0.33	SO_4	$R\bar{3}$	8
shigaite	Mn	2.00	0.33	SO_4	$R\bar{3}$	9
charmarite-2H	Mn	2.00	0.33	CO_3	$P6_322$	2
charmarite-3T	Mn	2.00	0.33	CO_3	$P3_12, P3_212$	2
zaccagnaite	Zn	2.00	0.33	CO_3	$P6_3/mmc$	10
zaccagnaite-3R	Zn	1.63	0.38	CO_3	$R\bar{3}m$	
glaucocerinite	Zn	1.63	0.38	SO_4, CO_3	Rhombohedral	11
zincowoodwardite-3R	Zn	2.00–1.00	0.33–0.50	SO_4	$R\bar{3}m$	12
zincowoodwardite-1T	Zn	2.00	0.33	SO_4	$P\bar{3}$	12
alvanite	Zn	0.25	0.80	VO_3	$P2_1/n$	13
woodwardite	Cu	2.00	0.33	SO_4	$R\bar{3}m$	14
hydrowoodwardite	Cu	>0.75	<0.67	SO_4	$R\bar{3}m$	15
cyanotrichite	Cu	2.00	0.33	SO_4	Orthorhombic	16
chalcoalumite	Cu	0.25	0.80	SO_4	$P2_1$	17
spangolite	Cu	6.07	0.14	SO_4, Cl	$P3_1c$	18
takovite	Ni	3.00	0.25	CO_3	$R\bar{3}m$	19
nickelalumite	Ni	0.25	0.80	SO_4, NO_3	$P2_1$	20
carrboydite	Ni	1.45	0.41	SO_4, CO_3	Hexagonal	21
mbobomkulite	Ni	0.25	0.80	SO_4, NO_3	Monoclinic	22
hydrombobomkulite	Ni	0.25	0.80	SO_4, NO_3	Monoclinic	22
ankinovichite	Ni	0.25	0.80	VO_3	$P2_1/n$	23

Notes: References: 1 = Manasse (1915); Frondel (1941). 2 = Chao and Gault (1997). 3 = Krivovichev et al. (2010b). 4 = Krivovichev et al. (2010a). 5 = Rodgers et al. (1977). 6 = Koritnig and Süssse (1975). 7 = Kashaev et al. (1982). 8 = Huminichi and Hawthorne (2003). 9 = Peacor et al. (1985). 10 = Merlino and Orlandi (2001). 11 = Raade et al. (1985). 12 = Witzke and Raade (2000). 13 = Pertlink and Dunn (1990). 14 = Nickel (1976). 15 = Witzke (1999). 16 = Palache et al. (1951). 17 = Larsen and Vassar (1925). 18 = Merlino et al. (1992). 19 = Bish and Brindley (1977). 20 = Uvarova et al. (2005). 21 = Nickel and Clarke (1976). 22 = Martini (1980a). 23 = Karpenko et al. (2004).

The El Soplao zaccagnaites-3R was formed as a secondary alteration product after biogenic Zn- and Al-rich ferro-manganese oxides. This origin is suggested by the regular presence of an alteration halo depleted in Zn and Al located between the zaccagnaites-3R crystals and the Zn-Al-rich ferromanganese oxides (Figs. 1d–1e). The observation that zaccagnaites-3R occurrence is limited to the stromatolite layers where the ferromanganese oxide material is richer in Zn (above 15 wt%) further supports that origin.

The El Soplao zaccagnaites-3R is speleothemic, i.e., it formed in the cave. This is because it is linked to the alteration of ferromanganese stromatolites, which were formed in a karstic cave stream passage, induced by Mn-oxidizing microbes, as showed by Rossi et al. (2010). Therefore, zaccagnaites represents a new cave mineral. Similar to zaccagnaites-3R, other hydroxalcalites have only been found in caves, such as mbobomkulite, hydrombobomkulite, or sveite (Martini 1980a, 1980b). The discovery of zaccagnaites-3R in the El Soplao cave confirms that some caves are potential places for the formation of hydroxalcalites.

The age of the studied zaccagnaites-3R is unknown. Its minimum age is the age of the hosting stromatolites, which are at least 1 Ma old, based on U-series dating of carbonate speleothems that postdate the stromatolites (Rossi et al. 2010). The El Soplao zaccagnaites-3R likely formed at low temperatures (≤ 11 °C). In caves, temperatures are rather constant and normally represent the mean annual temperatures in the land surface above the cave. Currently, the temperature in the cave passage that hosts the zaccagnaites-3R-bearing stromatolites is about 11 °C. Given that the Holocene is one of the warmest interglacials of the Quaternary, it is very likely that the current cave temperature is close to the maximum temperature of the last million years. Therefore, the El Soplao zaccagnaites-3R most likely precipitated at 11 °C or less.

ACKNOWLEDGMENTS

This work was supported by Grant-ICT-Soplao-53.5.00.12.00, co-funded by the Instituto Geológico y Minero de España, the provincial government of Cantabria, and Turismo del Nansa. Alfredo Fernández Larios and José E. Fernández Rubio are greatly acknowledged for assistance in the EMP and IR analyses, respectively. We thank Juan Antonio Martín Rubí and Eva Bellido (Tres Cantos Laboratory, IGME) for their support and assistance in the first identification of zaccagnaites. We also thank I. Rosales and F. Unzué for their support and encouragement during the course of this study. The comments and suggestions of R.L. Frost, S. Merlino, and an anonymous reviewer greatly improved the original manuscript.

REFERENCES CITED

- Adachi-Pagano, M., Forano, C., and Besse, J.P. (2003) Synthesis of Al-rich hydroxalcalite-like compounds by using the urea hydrolysis reaction-control of size and morphology. *Journal of Materials Chemistry*, 13, 1988–1993.
- Ashwal, L.D. and Cairncross, B. (1997) Mineralogy and origin of stichtite in chromite-bearing serpentinites. *Contributions to Mineralogy and Petrology*, 127, 75–86.
- Belsky, A., Hellenbrandt, M., Karen, V.L., and Luksch, P. (2002) New developments in the Inorganic Crystal Structure Database (ICSD): accessibility in support of materials research and design. *Acta Crystallographica*, B58, 364–369.
- Bish, D.L. and Brindley, G.W. (1977) A reinvestigation of takovite, a nickel aluminum hydroxyl-carbonate of the pyroaurite group. *American Mineralogist*, 62, 458–464.
- Bookin, A.S. and Drits, V.A. (1993) Polymorphism of the hydroxalcalite-like minerals. I. Possible polytypes and their diffraction features. *Clays and Clay Minerals*, 41, 551–557.
- Brindley, G.W. and Kikkawa, S. (1979) A crystal-chemical study of Mg, Al and Ni, Al hydroxyl-perchlorates and hydroxyl-carbonates. *American Mineralogist*, 64, 836–843.
- Chao, G.Y. and Gault, R.A. (1997) Quintinitite-2H, quintinitite-3T, charmarite-2H, charmarite-3T and caresite-3T, a new group of carbonate minerals related to the hydroxalcalite-manasseite group. *The Canadian Mineralogist*, 35, 1541–1549.
- Chen, H. and Zhang, W.G. (2010) A strong-fluorescent Tb-containing hydroxalcalite-like compound. *Journal of American Ceramic Society*, 93, 2305–2310.
- Dani, N., Formoso, M.L.L., Decarreau, A., and Meunier, A. (2001) Nordstrandite in bauxite derived from phonolite, Lages, Santa Catarina, Brazil. *Clays and Clay Minerals*, 49, 216–222.
- De Vaal, S.A. and Viljoen, E.A. (1971) Nickel minerals from Barberton, South-Africa. IV. Reevesite, a member of the hydroxalcalite group. *American Mineralogist*, 56, 1077–1081.
- del Hoyo, C. (2007) Layered double hydroxides and human health. An overview. *Applied Clay Science*, 36, 103–121.
- Douglas, G.B., Wendling, L.A., Pleysier, R., and Trefry, M.G. (2010) Hydroxalcalite formation for contaminant removal from Ranger Mine process water. *Mine Water and the Environment*, 29, 108–115.
- Drits, V.A., Sokolova, T.N., Sokolova, G.V., and Cherkashin, I. (1987) New members of the hydroxalcalite-manasseite group. *Clays and Clay Minerals*, 35, 401–417.
- Frondel, C. (1941) Constitution and polymorphism of the pyroaurite and sjögrenite groups. *American Mineralogist*, 26, 295–315.
- Frost, R.L. and Erickson, K. (2004) Vibrational spectroscopy of stichtite. *Spectrochimica Acta. Part A, Molecular and Biomolecular Spectroscopy*, 60, 3001–3005.
- Frost, R.L. and Reddy, B.J. (2006) Thermo-Raman spectroscopic study of the natural layered double hydroxide manasseite. *Spectrochimica Acta*, 65, 553–559.
- Frost, R.L., Martens, W.N., and Erickson, K.L. (2005) Thermal decomposition of the hydroxalcalite. Thermogravimetric analysis and hot stage Raman spectroscopic study. *Journal of Thermal Analysis and Calorimetry*, 82, 603–608.
- Frost, R.L., Dickfos, M.J., and Reddy, B.J. (2008) Raman spectroscopy of hydroxyl nickel carbonate minerals nullaginite and zaraitite. *Journal of Raman Spectroscopy*, 39, 1250–1256.
- He, J., Wei, M., Li, B., Kang, Y., Evans, D.G., and Duan, X. (2006) Preparation of layered double hydroxides. *Structure & Bonding*, 119, 89–119.
- Huminić, D.M.C. and Hawthorne, F.C. (2003) The crystal structure of nikischierite, $\text{NaFe}_2^+\text{Al}_3(\text{SO}_4)_2(\text{OH})_{18}(\text{H}_2\text{O})_{12}$, a mineral of the shigaite group. *The Canadian Mineralogist*, 41, 79–82.
- Karpenko, V.Y., Pautov, L.A., Sokolova, E.V., Hawthorne, F.G., Agakhanov, A.A., Dikaya, T.V., and Bekenova, G.K. (2004) Ankinovichite, the nickel analogue of alvanite, a new mineral from Kurumsak (Kazakhstan) and Kara-Chagyr (Krygyzstan). *Zapiski Vsesoyuznogo Mineralogicheskogo Obshchestva*, 133, 59–70.
- Kashaev, A.A., Feoktistov, G.D., and Petrova, S.V. (1982) Chlormagaluminite, $(\text{Mg}, \text{Fe}^{2+})_4\text{Al}_2(\text{OH})_{12}(\text{Cl}, 12\text{CO}_3)_2 \cdot 2\text{H}_2\text{O}$, a new mineral of the manasseite-sjögrenite group. *Zapiski Vsesoyuznogo Mineralogicheskogo Obshchestva*, 11, 121–127.
- Kloprogge, J.T. and Frost, R.L. (1999) Fourier transform infrared and Raman spectroscopic study of the local structure of Mg-, Ni-, and Co-hydroxalcalites. *Journal of Solid State Chemistry*, 146, 506–515.
- Kloprogge, J.T., Hickey, L., and Frost, R.L. (2004) The effects of synthesis pH and hydrothermal treatment on the formation of zinc aluminum hydroxalcalites. *Journal of Solid State Chemistry*, 177, 4047.
- Koritnig, S. and Süss, P. (1975) Meixnerite, $\text{Mg}_6\text{Al}_2(\text{OH})_{18} \cdot 4\text{H}_2\text{O}$, ein neues Magnesium-Aluminium-Hydroxid-Mineral. *Tschermak's Mineralogisch-Petrographische Mitteilungen*, 22, 79–87.
- Kovács-Pálffy, P., Velledits, F., Kónya, P., Földvári, M., and Sólymos, K.G. (2008) Nordstrandite, a new occurrence from Hungary. *Acta Mineralogica-Petrographica*, 48, 43–48.
- Krivovichev, S.V., Yakovenchuk, V.N., Zhitova, E.S., Zolotarev, A.A., Pakhomovsky, Y.A., and Ivanyuk, G.Y. (2010a) Crystal chemistry of natural layered double hydroxides. 2. Quintinitite-1M: first evidence of a monoclinic polytype in $\text{M}^{2+}\text{-M}^{3+}$ layered double hydroxides. *Mineralogical Magazine*, 74, 833–840.
- Krivovichev, S.V., Yakovenchuk, V.N., Zhitova, E.S., Zolotarev, A.A., Pakhomovsky, Y.A., and Ivanyuk, G.Y. (2010b) Crystal chemistry of natural layered double hydroxides. 1. Quintinitite-2H-3c from the Kovdor alkaline massif, Kola peninsula, Russia. *Mineralogical Magazine*, 74, 821–832.
- Larsen, E.S. and Vassar, H.E. (1925) Chalcoalumite, a new mineral from Bisbee, Arizona. *American Mineralogist*, 10, 79–83.
- Lombardo, G.M., Pappalardo, G.C., Punzo, F., Costantino, F., Costantino, U., and Sisani, M. (2005) A novel integrated X-ray powder diffraction (XRPD) and molecular dynamics (MD) approach for modelling mixed-metal (Zn, Al) layered double hydroxides (LDHs). *European Journal of Inorganic Chemistry*, 24, 5026–5034.
- Manasse, E. (1915) Idrotalcite e piroaurite. *Atti della Società Toscana di Scienze Naturali*, 24, 92–105.
- Martini, J.E.J. (1980a) Mbobomkulite, hydrombobomkulite and nickellalumite, new minerals from Mbobo Mkuulu cave, Eastern Transvaal. *Annals of Geological Survey of South Africa*, 14, 1–10.
- (1980b) Sveite, a new mineral from Autana Cave, Territorio federal Amázonas, Venezuela. *Transactions of the Geological Society of South Africa*,

- 83, 239–241.
- Merlino, S. and Orlandi, P. (2001) Carraraite and zaccagnaite, two new minerals from the Carrara marble quarries: their chemical compositions, physical properties, and structural features. *American Mineralogist*, 86, 1293–1301.
- Merlino, S., Pasero, M., Sabelli, C., and Trosti-Ferroni, R. (1992) Crystal structure refinements of spangolite, a hydrated basic sulphate of copper and aluminum, from three different occurrences. *Neues Jahrbuch für Mineralogie Monatshefte*, H, 8, 349–357.
- Nickel, E. (1976) New data on woodwardite. *Mineralogical Magazine*, 43, 644–647.
- Nickel, E.H. and Clarke, R.M. (1976) Carrboydite, a hydrated sulfate of nickel and aluminum: a new mineral from Western Australia. *American Mineralogist*, 61, 366–372.
- Othman, M.R., Helwani, Z., Martunus, M., and Fernando, W.J.N. (2009) Synthetic hydroxaltes from different routes and their application as catalysts and gas adsorbents: a review. *Applied Organometallic Chemistry*, 23, 335–346.
- Palache, C., Berman, H., and Frondel, C. (1951) *Dana's System of Mineralogy*, (7th edition), vol. II, 578–579. Wiley, New York.
- Peacor, D.R., Dunn, P.J., Kato, A. and Wicks, F.J. (1985) Shigaite, a new manganese aluminum sulfate mineral from the Ioi mine, Shiga, Japan. *Neues Jahrbuch für Mineralogie Monatshefte*, 453–457.
- Pertlink, F. and Dunn, P.J. (1990) Crystal structure of alvanite, $(\text{Zn,Ni})\text{Al}_4(\text{VO}_3)_2(\text{OH})_{12}\cdot 2\text{H}_2\text{O}$, the first example of an unbranched zweier-single chain vanadate in nature. *Neues Jahrbuch für Mineralogie, Monatshefte*, 385–392.
- Raade, G., Elliott, C.J., and Din, V.K. (1985) New data on glaucocerinite. *Mineralogical Magazine*, 49, 583–590.
- Ramseyer, K., Miano, T.M., D'Orazio, V., Wildberger, A., Wagner, T., and Geister, J. (1997) Nature and origin of organic matter in carbonates from speleothems, marine cements and coral skeletons. *Organic Geochemistry*, 26, 361–378.
- Rietveld, H.M. (1967) Line profiles of neutron powder-diffraction peaks for structure refinement. *Acta Crystallographica*, 22, 151–152.
- (1969) A profile refinement method for nuclear and magnetic structures. *Journal of Applied Crystallography*, 2, 65–71.
- Rodgers, K.A., Chisholm, J.E., Davis, R.J., and Nelson, C.S. (1977) Motukoreaite, a new hydrated carbonate, sulphate, and hydroxide of Mg and Al from Auckland, New Zealand. *Mineralogical Magazine*, 41, 389–390.
- Rodríguez-Carvajal, J. (1993) Recent advances in magnetic structure determination by neutron powder diffraction. *Physica B*, 192, 55–69.
- Rossi, C., Lozano, R.P., Isanta, N., and Hellstrom, J. (2010) Manganese stromatolites in caves: El Soplao (Cantabria, Spain). *Geology*, 12, 1119–1122.
- Roto, R., Nindiyasari, F., and Tahir, I. (2009) Removal of hexacyanoferrate(II) using Zn-Al-O-Ac Hydroxaltes as an anion exchanger. *Journal of Physical Science*, 20, 73–84.
- Stumpf, T., Curtius, H., Walther, C., Dardenne, K., Ufer, K., and Fanghanel, T. (2007) Incorporation of Eu(III) into hydroxaltes: a TRLS and EXAFS study. *Environmental Science & Technology*, 41, 3186–3191.
- Su, J., Dong, F., Zhang, M., and Zhang, S. (2011) Fluorescent properties of Zn-Al hydroxaltes and its modified products. *Advanced Materials Research*, 148–149, 1087–1090.
- Taylor, H.F.W. (1973) Crystal structures of some double hydroxide minerals. *Mineralogical Magazine*, 39, 377–389.
- Taylor, R.M., Hansen, H.C.B., Satnger, G., and Bender-Koch, C. (1991) On the genesis and composition of natural pyroaurite. *Clay Minerals*, 26, 297–309.
- Temuujin, J., Jadambaa, T.S., Mackenzie, K.J.D., Angerer, A., Porte, F. and Riley, F. (2000) Thermal formation of corundum from aluminium hydroxides prepared from various aluminium salts. *Bulletin of Material Science*, 23, 301–304.
- Thevenot, F., Szymanski, R., and Chaumette, P. (1989) Preparation and characterization of Al-rich Zn-Al hydroxaltes-like compounds. *Clays and Clay Minerals*, 37, 396–402.
- Trave, A., Selloni, A., Goursot, A., Tichit, D., and Weber, J. (2002) First principles study of the structure and chemistry of Mg-based hydroxaltes-like anionic clays. *Journal of Physical Chemistry B*, 106, 12291–12296.
- Tumiaiti, S., Godard, G., Masciocchi, N., Martin, S., and Monticelli, D. (2008) Environmental factors controlling the precipitation of Cu-bearing hydroxaltes-like compounds from mine waters. The case of the “*Eve-verda*” spring (Aosta Valley, Italy). *European Journal of Mineralogy*, 20, 73–94.
- Uvarova, Y.A., Sokolova, E., Hawthorne, F.C., Karpenko, V.V., Agakhanov, A., and Pautov, L.A. (2005) The crystal chemistry of the “nickelalumite”-group minerals. *The Canadian Mineralogist*, 43, 1511–1519.
- van Beynen, P., Bourbonniere, R., Ford, D., and Schwarcz, H. (2001) Causes of colour and fluorescence in speleothems. *Chemical Geology*, 175, 319–341.
- Vieira, A.C., Moreira, R.L., and Dias, A. (2009) Raman scattering and Fourier transform infrared spectroscopy of $\text{Me}_2\text{Al}_2(\text{OH})_6\text{Cl}_2\cdot 4\text{H}_2\text{O}$ (Me=Mg, Ni, Zn, Co, and Mn) and $\text{Ca}_2\text{Al}(\text{OH})_6\text{Cl}_2\cdot 2\text{H}_2\text{O}$ hydroxaltes. *Journal of Physical Chemistry C*, 113, 13358–13368.
- Wang, J., Kalinichev, A.G., Amonette, J.E., and Kirkpatrick, R.J. (2003) Interlayer structure and dynamics of Cl-bearing hydroxaltes: far infrared spectroscopy and molecular dynamics modeling. *American Mineralogist*, 88, 398–409.
- Witzke, T. (1999) Hydroxaltes, a new mineral of the hydroxaltes group from Königswalde near Annaberg, Saxony/Germany and other localities. *Neues Jahrbuch für Mineralogie Monatshefte*, 2, 75–86.
- Witzke, T. and Raade, G. (2000) Zincwoodwardite, $[\text{Zn}_{1-x}\text{Al}_x(\text{OH})_2][(\text{SO}_4)_{0.2}(\text{H}_2\text{O})_m]$, a new mineral of the hydroxaltes group. *Neues Jahrbuch für Mineralogie Monatshefte*, 455–465.
- Zamarreño, I., Plana, F., Vazquez, A., and Clage, D.A. (1989) Motukoreaite: a common alteration product in submarine basalts. *American Mineralogist*, 74, 1054–1058.
- Zhao, Y., Li, F., Zhang, R., Evans, D.G., and Duan, X. (2002) Preparation of layered double-hydroxide nanomaterials with a uniform crystallite size using a new method involving separate nucleation and aging steps. *Chemistry of Materials*, 14, 4286–4291.
- Zhitova, E.S., Yakovenchuk, V.N., Krivovichev, S.V., Zolotarev, A.A., Pakhomovsky, Y.A., and Ivanyuk, G.Y. (2010) Crystal chemistry of natural layered double hydroxides. 3. The crystal structure of Mg, Al-disordered quintinite-2H. *Mineralogical Magazine*, 74, 841–848.

MANUSCRIPT RECEIVED JUNE 8, 2011

MANUSCRIPT ACCEPTED DECEMBER 18, 2011

MANUSCRIPT HANDLED BY HONGWU XU